Chemistry on the Edge: A Microscopic Analysis of the Intercalation, Exfoliation, Edge Functionalization, and Monolayer Surface Tiling Reactions of α-Zirconium Phosphate

David M. Kaschak,[†] Stacy A. Johnson,[†] Daniel E. Hooks,[‡] Hyuk-Nyun Kim,[†] Michael D. Ward,*[,‡] and Thomas E. Mallouk*[,†]

Contribution from the Department of Chemistry, Pennsylvania State University, University Park, Pennsylvania 16802, and Department of Chemical Engineering and Materials Science, University of Minnesota, Minneapolis, Minnesota 55455

Received May 29, 1998

Abstract: The intercalation and exfoliation reactions of α-zirconium phosphate, $Zr(HPO_4)_2 \cdot H_2O$ (α-ZrP), were studied microscopically by atomic force microscopy (AFM) and transmission electron microscopy (TEM). The reaction of α-ZrP with tetra(*n*-butylammonium) hydroxide (TBA^+OH^-) initially produces intercalation compounds, which then transform to unilamellar colloids. The rate-determining step in intercalation is the opening of the interlamellar galleries. Subsequent diffusion of TBA^+ ions into the opened galleries is rapid. The hydrolysis reaction of α-ZrP colloids proceeds from the edges inward, forming ∼4-nm hydrated zirconia particles that decorate the edges of the sheets. The reaction does not go to completion, as it is limited by equilibrium associated with the release of phosphate into the solution. The hydrolysis reaction is negligible at 0 °C, which permits the synthesis of hydrolysis-free unilamellar colloids. Remarkably, these colloids form monolayer films on amine-derivatized silicon surfaces with a high density that suggests significant surface mobility during the adsorption process. Addition of appropriate phosphonic acids to colloidal α-ZrP suspensions enables modification of the sheet edges, illustrated here by the anchoring of osmium oxide particles to the sheet edges by a vinylphosphonate linker.

Introduction

Lamellar compounds, materials with strong bonds in two dimensions and weak bonds in the third, commonly undergo two kinds of topochemical reactions. Intercalation reactions occur with retention of the two-dimensional bonding, with interlayer galleries opened to admit guest molecules. The solid remains crystalline or semicrystalline because of attractive interactions between the guest and flanking sheets of the host. The second type of reaction—exfoliation—can be considered an extreme case of intercalation in which the forces between the sheets are weakly attractive or even repulsive. Consequently, the sheets can be easily separated by solvent molecules to form discrete lamellae.[1] These lamellar colloids can be restacked to make the parent solid or its intercalation compounds. This feature has prompted their use as precursors for polymer-sheet nanocomposites[2] and self-assembled aperiodic multilayers.[3]

The exfoliation of clays, alkali transition metal oxides, metal phosphates, graphite oxide, layered double hydroxides, and lamellar chalcogenides yields unilamellar colloids and, under some conditions, dimers and higher aggregates of individual sheets.[4] These lamellar colloids have large basal planes and thin edges, resulting in two distinct atomic environments. Individual particles typically have thicknesses of <2 nm such that the edge region can be described as a "molecular line". Surprisingly, there have been few experiments that probe and compare the chemical reactivities of these two regions.[5]

We describe herein the examination of a widely used unilamellar colloid derived from α-zirconium phosphate (α-ZrP), $Zr(HPO_4)_2 \cdot H_2O$.[6] This colloid has been studied as a building block of supramolecular assemblies,[7] thin films,[8] and membranes[9] and is the parent compound of many organic derivatives.[10] Some of these studies have demonstrated that

[†] Pennsylvania State University.

[‡] University of Minnesota.

(1) (a) Jacobson, A. J. *Mater. Sci. Forum* **1994**, *152*−*153*, 1. (b) Jacobson, A. J. In *Comprehensive Supramolecular Chemistry*; Alberti, G., Bein, T., Eds.; Elsevier: Oxford, UK, 1996; Vol. 7, pp 315−335.

(2) (a) Krishnamoorti, R.; Vaia, R. A.; Giannelis, E. *Chem. Mater.* **1996**, *8*, 1728. (b) Lemmon, J. P.; Lerner, M. M. *Chem. Mater.* **1994**, *6*, 207. (c) Tsai, H.-L.; Heising, J.; Schindler, J. L.; Kannewurf, C. R.; Kanatzidis, M. G. *Chem. Mater.* **1997**, *9*, 879. (d) Tsai, H.-L.; Schindler, J. L.; Kannewurf, C. R.; Kanatzidis, M. G. *Chem. Mater.* **1997**, *9*, 875.

(3) (a) Kleinfeld, E. R.; Ferguson, G. S. *Science* **1994**, *265*, 370. (b) Kleinfeld, E. R.; Ferguson, G. S. *Chem. Mater.* **1995**, *7*, 2329. (c) Kotov, N. A.; Dekany, I.; Fendler, J. H. *Adv. Mater.* **1996**, *8*, 637. (d) Lvov, Y.; Ariga, K.; Kunitake, T. *J. Am. Chem. Soc.* **1995**, *117*, 6117. (e) Mallouk, T. E.; Kim, H.-N.; Ollivier, P. J.; Keller, S. W. In *Comprehensive Supramolecular Chemistry*; Alberti, G., Bein, T., Eds.; Elsevier: Oxford, UK, 1996; Vol 7, pp 189−217.

(4) Sasaki, T.; Watanabe, M.; Hashizume, H.; Yamada, H.; Nakazawa, H. *J. Am. Chem. Soc.* **1996**, *118*, 8329.

(5) (a) Thiessen, P. A. Z. *Elektrochem.* **1942**, *48*, 675. (b) Thiessen, P. A. *Z. Anorg. Chem.* **1947**, *253*, 161. (c) van Olphen, H. *An Introduction to Clay Colloid Chemistry*; John Wiley & Sons: New York, 1963; pp 92−95.

(6) (a) Alberti, G. *Acc. Chem. Res.* **1978**, *11*, 163. (b) Clearfield, A. *Chem. Rev.* **1988**, *88*, 125.

(7) (a) Mallouk, T. E.; Gavin, J. A. *Acc. Chem. Res.* **1998**, *31*, 209. (b) Brunet, E.; Huelva, M.; Rodriguez-Ubis, J. C. *Tetrahedron Lett.* **1994,** *35*, 8697. (c) Alberti, G.; Costantino, U.; Dionigi, C.; Murcia-Mascarós, S.; Vivani, R. *Supramol. Chem.* **1995**, *6*, 29. (d) Alberti, G.; Boccali, L.; Dionigi, C.; Vivani, R.; Kalchenko, V. I.; Atamas, L. I. *Supramol. Chem.* **1996**, *7*, 129. (e) Brunet, E.; Huelva, M.; Vazquez, R.; Olga, J.; Rodriguez-Ubis, J. C. *Chem. Eur. J.* **1996**, *2*, 1578. (f) Zhang, B.; Clearfield, A. *J. Am. Chem. Soc.* **1997**, *119*, 2751. (g) Ding, Y.; Jones, D. J.; Maireles-Torres, P.; Roziere, J. *Chem. Mater.* **1995**, *7*, 562. (h) Kumar, C. V.; McLendon, G. L. *Chem. Mater.* **1997**, *9*, 863.

10.1021/ja9818710 CCC: $15.00
Published on Web 10/01/1998

the intercalation/exfoliation of lamellar metal phosphates is a consequence of a base hydrolysis reaction that partially (or completely) destroys the sheets.[11] We demonstrate here that base hydrolysis occurs exclusively at the *edges* of the α-ZrP sheets, where hydrolyzable phosphate groups are most accessible. The activation energy for hydrolysis is greater than that for intercalation/exfoliation, which results in a substantial dependence of the outcome of the reaction on temperature. The intercalation/exfoliation processes can be examined in microscopic detail at low temperature without the complication of hydrolysis. This permits the formation of self-assembled monolayers of non-hydrolyzed sheets that efficiently tile cationic surfaces. We also demonstrate that the hydrolysis reaction is an equilibrium process that may be slowed dramatically by adding phosphate (the reaction product) to basic colloidal suspensions. This dynamic equilibrium can be exploited to derivatize α-ZrP colloids exclusively at the sheet edges with organophosphonates.

Experimental Section

Materials. The α-ZrP was prepared as described in a previous study.[8a] The semicrystalline material was synthesized by refluxing in phosphoric acid for 2 days, and the microcrystalline product was obtained after precipitation for 7 days. Vinylphosphonic acid (97%), tetra(*n*-butylammonium) hydroxide (40%), osmium tetraoxide (4%), and ammonium molybdate were used as received (Aldrich Chemical Co.). Phosphomolybdic acid (Fisher Scientific), ethylphosphonic acid (98%, Aldrich), and (4-aminobutyl)dimethylmethoxysilane (United Chemical Technologies) were also used as received.

Exfoliation of α-Zr(HPO$_4$)$_2$·H$_2$O (α-ZrP). Colloidal suspensions of α-ZrP were prepared by adding 1.24×10^{-4} mol of tetra(*n*-butylammonium) hydroxide (TBA^+OH^-) to 1.66×10^{-4} mol of α-ZrP in 25 mL of Nanopure water. The progress of the hydrolysis reaction was measured by varying incubation times between 15 min and 12 h. Exfoliation temperatures were varied between 0 and 75 °C.

ICP-AES and Phosphomolybdic Acid Determination of Zr and P. Two drops of 37% HCl were added to a 5-mL aliquot of each colloidal suspension to precipitate the α-ZrP sheets and solid products of the hydrolysis reaction. The restacked solids were collected by centrifugation and reacted with 15 mL of 1% HF to give clear solutions. The P/Zr ratio of the resulting solution was determined using a Leeman Labs PS3000UV inductively coupled argon plasma atomic emission spectrometer (ICP-AES).

The concentration of free orthophosphate ions in the solution was determined by the method of Bernhart and Wreath.[12] To 20 mL of the supernatant solution was added 10 mL of 30 mM ammonium molybdate. After 10 min, the yellow phosphomolybdic acid precipitate was collected by centrifugation, dissolved in acetone, and quantified by means of its 330-nm absorption band, using a Hewlett-Packard 8452A diode array spectrophotometer. An extinction coefficient of 33 400 $M^{-1}cm^{-1}$ at 330 nm was calculated from a Beer's law plot of phosphomolybdic acid isolated by this method. This is within experimental error of the 37 400 $M^{-1}\,cm^{-1}$ value derived from the same plot obtained from phosphomolybdic acid purchased from Fisher Scientific.

Acid Titration of a Unilamellar α-ZrP Colloid. α-ZrP (0.053 g; 1.76×10^{-4} equiv) was suspended in 25 mL of Nanopure water at 0 °C. TBA^+OH^- was added (2.56×10^{-4} mol), and the suspension was stirred for 1 h. Aqueous HCl (0.122 M) was added dropwise, and the pH was monitored using an Orion model 420A pH meter. The titration was performed slowly (3 h total) in order to allow adequate time for equilibration in the restacking process.

Silicon Substrate Preparation. Samples were cut from polished Si (100) wafers, sonicated in CCl_4 for 15 min, and rinsed with methanol and water. The samples were then sonicated in piranha solution (2:1 mixture of concentrated H_2SO_4:30% H_2O_2) for ca. 30 min and rinsed with water. They were then rinsed with methanol, methanol/toluene (1:1), and toluene before being placed in a 0.05 wt % solution of (4-aminobutyl)dimethylmethoxysilane in toluene overnight. The samples were rinsed with toluene, methanol/toluene (1:1), methanol, and water and were then immediately immersed into the α-ZrP suspension.

α-ZrP Edge Derivatization. Typically, 2.6×10^{-4} mol of vinylphosphonic acid (or 2.7×10^{-4} mol of ethylphosphonic acid) was dissolved in 25 mL of Nanopure water with ca. 2.1×10^{-4} mol of TBA^+OH^- and 1.16×10^{-4} mol of α-ZrP. Additional base (ca. 2×10^{-4} mol) was added to compensate for the acidity of the added phosphonates, increasing the pH to ∼11. This solution was incubated at room temperature for 2 h to allow exchange of phosphates, 2.3×10^{-5} mol of OsO_4 was added, and the solution was incubated an additional 20 min. The TEM samples were prepared immediately as described below.

TEM. Transmission electron microscope images were obtained with a JEOL 1200 EXII at 120 kV of accelerating voltage and 75−80 mA of filament current. Samples were made by swirling a Formvar-coated, 200-mesh copper grid through the reaction solution two times and then dipping it into a flask of DI water for 1 s. The grid was shaken to remove excess water, air-dried, and then placed in a desiccator. All samples were stored in a desiccator for at least 15 h and then stored under reduced pressure (∼200 mTorr) for 15 min directly before they were transferred into the TEM instrument.

Atomic Force Microscopy (AFM). AFM images were obtained using a Digital Instruments (Santa Barbara, CA) NanoScope III multimode scanning probe microscope equipped for operation in liquid, with a scan head having a maximum range of 15 μm × 15 μm. AFM probes (Digital Instruments, Santa Barbara, CA) consisted of triangular silicon nitride cantilevers (force constant = 0.06 N m^{-1}) with integral pyramidal tips.

Hydrothermally grown α-ZrP crystals[13] were mounted on steel disks using an epoxy cured by UV exposure (Summers Laboratories Optical Division, Fort Washington, PA). The entire area of the disk was coated with this epoxy to reduce the chance of solution contamination by corrosion products of the steel upon exposure to the liquid environment. Molecular contrast AFM images were acquired in contact mode under nominally constant force conditions, with line scan rates of 20−30 Hz and 512 × 512 pixel data collection. The tip−sample force was minimized before imaging by reducing the set point to a value just below tip disengagement. The α-ZrP surface was imaged in water prior to addition of intercalant solutions. Intercalation experiments with TBA^+OH^- were performed both while scanning and with the tip retracted. AFM images of α-ZrP thin films were obtained at lower resolution in tapping mode, using a 3045JVW piezo tube scanner. The 125-μm etched silicon cantilevers had a resonant frequency between 250 and 325 kHz, and the oscillation frequency for scanning was set to ∼0.1−3 kHz below resonance. Typical images were obtained at line scan rates of 2 Hz while collecting 256 × 256 pixel samples.

Results and Discussion

AFM Imaging of α-ZrP Crystals and the Early Stages of Intercalation. AFM imaging of the basal planes of large ($1 \times 0.5 \times 0.055$ mm and $0.8 \times 0.4 \times 0.018$ mm) α-ZrP crystals immersed in deionized water reveals a very well ordered structure (Figure 1). The surface lattice parameters measured by Fourier analysis of the AFM images ($a = 9.8 \pm 0.35$ Å, *b*

(8) (a) Keller, S. W.; Kim, H.-N.; Mallouk, T. E. *J. Am. Chem. Soc.* **1994**, *116*, 8817. (b) Kaschak, D. M.; Mallouk, T. E. *J. Am. Chem. Soc.* **1996**, *118*, 4222. (c) Fang, M.; Kaschak, D. M.; Sutorik, A. C.; Mallouk, T. E. *J. Am. Chem. Soc.* **1997**, *119*, 12184.

(9) (a) Alberti, G.; Casciola, M.; Costantino, U. *J. Colloid Interface Sci.* **1985**, *107*, 256. (b) Alberti, G.; Casciola, M.; Costantino, U.; Di Gregorio, F. *Solid State Ionics* **1989**, *32/33*, 40. (c) Alberti, G.; Casciola, M.; Palombari, R. *Solid State Ionics* **1993**, *61*, 241.

(10) (a) Cao, G.; Hong, H.-G.; Mallouk, T. E. *Acc. Chem. Res.* **1992**, *25*, 420. (b) Thompson, M. E. *Chem. Mater.* **1994**, *6*, 1168. (c) Katz, H. E. *Chem. Mater.* **1994**, *6*, 2227. (d) Clearfield, A. in *Progress in Inorganic Chemistry*; Karlin, K. D., Ed.; John Wiley & Sons: New York, 1998; Vol. 47, pp 371−510.

(11) Alberti, G.; Marmottini, F. *J. Colloid Interface Sci.* **1993**, 157, 513.

(12) (a) Bernhart, D. N.; Wreath, A. R. *Anal. Chem.* **1955**, *27*, 440. (b) Netherton, L. E.; Wreath, A. R.; Bernhart, D. N. *Anal. Chem.* **1955**, *27*, 860.

(13) Alberti, G.; Torracca, E. *J. Inorg. Nucl. Chem.* **1968**, *30*, 317.

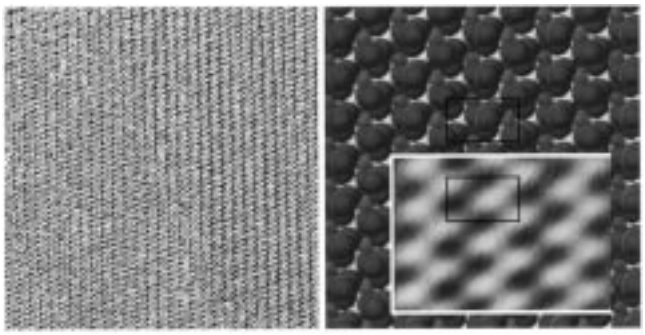

Figure 1. Unfiltered 20- × 20-nm AFM image (left) of the α-ZrP surface, and a space-filling model of the surface with superimposed filtered and zoomed data (right). The box on both the space-filling model and the filtered data corresponds to lattice parameters determined by X-ray diffraction.

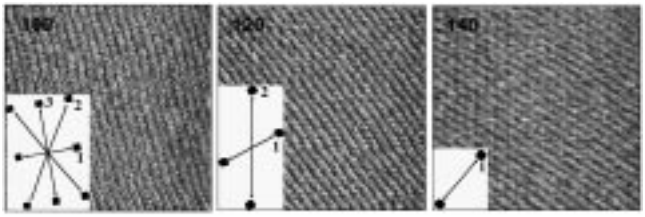

Figure 2. AFM images (20 × 20 nm) of α-ZrP at scan angles rotated in 20° increments, with corresponding Fourier transforms below each. Note that the different scan angles, given in the upper left of each image, result in different transforms (a 90° scan angle corresponds to a tip scan direction perpendicular to the cantilever). Transform spots, labeled 1, 2, and 3 in each inset (corresponding to lattices periodicities of 9.8, 5.3, and 6.0 Å, respectively; spots 2 and 3 are 60° and 90°, respectively, from spot 1), disappear in pairs with each 20° rotation. The transforms have been digitally enhanced for clarity.

$= 6.0 \pm 0.4$ Å, $g = 89.8 \pm 5.4°$) agree reasonably with those determined by X-ray powder diffraction ($a = 9.10$ Å, $b = 5.298$ Å, $g = 90°$).[14]

Fourier transforms of many images taken at a variety of scan angles revealed that, for some tips, the number of frequency components differed for different scan angles. For example, in the series of images depicted in Figure 2, successive scan angle rotations of 20° resulted in the disappearance of the Fourier spots corresponding to two lattice directions. This indicates that determination of surface lattice parameters should be performed at several different scan angles as a precaution. Although there have been reports of frictional anisotropy observed by the AFM on a larger scale,[15] to our knowledge this anisotropic scanning artifact has not been previously noted for atomic contrast AFM imaging.

Intercalation of α-ZrP (and other layered solids) involves the entry of intercalant molecules at the edges of the crystal followed by inward diffusion along the interlamellar galleries, as has been confirmed by microscopy of crystallites undergoing intercalation.[16,17] While other studies, including in situ X-ray diffraction,[18] have measured intercalation rates, these data represent an average of a large number of crystallites, not selected regions of a single crystal. This prompted us to use AFM, which allows examination of intercalation locally and in real time.

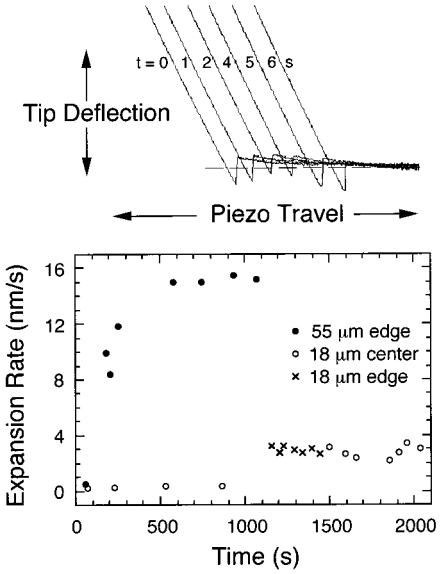

Figure 3. (Top) In situ contact-mode AFM force/distance curves from the basal plane of an α-ZrP crystal in the initial stage of the intercalation reaction with TBA^+OH^-. Movement of the whole force curve to the right (decreasing *z*-axis piezo travel) corresponds to crystal expansion. (Bottom) Expansion rate vs time for a 55-μm-thick crystal measured near the edge (●) and an 18-μm-thick crystal measured first near the center (○), and then near the edge (×).

The rates of crystal expansion normal to the basal plane resulting from intercalation were obtained by monitoring the change in AFM force curves at various points along the surface of hydrothermally grown single crystals of α-ZrP. The engagement and disengagement points on the force curves, which were constant under deionized water, moved monotonically to smaller values of *z*-axis piezo travel upon addition of 2×10^{-4} M TBA^+OH^- to the solution. This behavior is indicative of increasing crystal height during intercalation. Figure 3 depicts representative force curves acquired at approximately 1-s intervals.

This concentration was chosen to restrict the expansion rate to values that allowed for data acquisition on the AFM time scale. We have observed that the expansion rate is highly sensitive to the TBA^+OH^- concentration, with only a 2-fold increase over the aforementioned value resulting in rates that were too rapid for reliable measurement. Conversely, low concentrations result in negligible expansion rates.

Crystal expansion was measured in three locations, the first near the edge of a 55-μm-thick crystal (∼50 μm from the edge), the second near the center of an 18-μm-crystal (∼200 μm from the edge), and the third near the edge of the same 18-μm-crystal (∼50 μm from the edge). The instantaneous expansion rate was calculated from the distance traveled per unit time between two consecutive force curves. Each point in Figure 3 represents a running average of five instantaneous rates. Zero time corresponds to a scan taken immediately after the deionized water surrounding the crystal was replaced by the TBA^+OH^- solution. Missing data points correspond to times when scan parameters needed to be changed, or when the tip was repositioned on the crystal. The expansion rate was negligible at very early times (<60 s) for measurements near the edge of the thick crystal. Thereafter, the rate rose quickly, attaining a steady value of 15 nm/s after about 500 s. In contrast, the expansion rate was negligible for a much longer time at the

(14) Troup, J. M.; Clearfield, A. *Inorg. Chem.* **1977**, *16*, 3311.
(15) (a) Last, J. A.; Ward, M. D. *Adv. Mater* **1996**, *8*, 730. (b) Nisman, R.; Smith, P.; Vansco, G. J. *Langmuir* **1994**, *10*, 1667. (c) Fujisawa, S.; Sugawara, K.; Morita, S. *J. Vac. Sci. Technol. B* **1994**, *12*, 1635.
(16) (a) Chianelli, R. R. *J. Crystal Growth* **1976**, *34*, 329. (b) Chianelli, R. R.; Scanlon, J. C.; Rao, B. M. L. *J. Solid State Chem.* **1979**, *29*, 323.
(17) McKelvy, M.; Sidorov, M.; Marie, A.; Sharma, R.; Glaunsinger, W. *Chem. Mater.* **1994**, *6*, 2233.
(18) Price, S. J.; Evans, J. S. O.; Francis, R. J.; O'Hare, D. *Adv. Mater.* **1996**, *8*, 582.

center of the 18-μm crystal, with an expansion rate of 3.5 nm/s achieved only after 900 s (there is some uncertainty in this time because the tip was repositioned during the time interval between 900 and 1500 s).

The normalized expansion rates, obtained by dividing the measured rates by crystal thickness, agreed within experimental error and yielded an intercalation rate of 2×10^{-4} s^{-1} for both crystals. This demonstrates that the expansion rate scales with the number of α-ZrP layers. The TBA^+ diffusion rate within the interlamellar galleries can be estimated from the time required to achieve a constant expansion rate and the distance traveled in this time. Using the difference between the times at which a constant expansion rate was achieved at 50 and 200 μm for the two crystals ($\Delta x = 150$ μm, $\Delta t_1 = 1000$ s), we estimate a diffusion coefficient of $D = 2 \times 10^{-7}$ cm^2/s, assuming $D = \Delta x^2/\Delta t$. Diffusion coefficients calculated from the distance from the edge and the time required for constant expansion rates from zero time ($\Delta t_2 = 500$ s, $\Delta t_3 = 1500$ s) were 0.5×10^{-7} and 2.7×10^{-7} cm^2/s for the 18- and 55-μm crystals, respectively.

The measured intercalation rate is consistent with a first-order process that depends on opening interlayer galleries at the edge of the crystal. This behavior is consistent with the Avrami kinetic model that has been used previously to describe the intercalation of layered metal chalcogenides.[18] At low conversion (as in the present case, in which the intercalation reaction is 10−30% complete after 2000 s), the Avrami model predicts the observed constant reaction rate.[19] Physically, this means that the nucleation points of the solid-state reaction (i.e., opening of a gallery at the edge of the crystal) are well-separated and, therefore, noninteracting at low conversion.

Microscopic Characterization of α-ZrP Colloids. Brønsted bases intercalate α-ZrP by neutralizing interlamellar P−OH groups, and some, such as methylamine and *n*-propylamine, exfoliate the solid to make colloidal suspensions.[20] In the case of strong bases with large cations, such as TBA^+OH^-, the reaction proceeds in two stages, by first intercalating and then exfoliating α-ZrP.[21] In all cases, these reactions occur in competition with base hydrolysis, according to

$$Zr(HPO_4)_2 \cdot H_2O + nH_2O + 2yOH^- \rightarrow Zr(HPO_4)_{2-y}(OH)_{2y} + (1+n)H_2O + yHPO_4^{2-} \quad (1)$$

Most strategies for minimizing hydrolysis involve limiting the amount of base or the reaction time. It has generally been accepted that hydrolysis is inevitable in the exfoliation reaction and that, among the isostructural tetravalent metal phosphates, the stability toward hydrolysis decreases in the order ZrP ≫ TiP > SnP > PbP ≫ GeP.[20] However, little is known about this process mechanistically. Topotactic reactions of γ-ZrP[22] have recently been postulated to occur from the edges inward, yet the possibility of exclusive edge reactions of related colloids has not been discussed. It has been proposed that hydrolysis occurs on the basal plane surface of α-ZrP crystals and that, for this reason, the hydrolysis of colloids is more rapid than that of bulk intercalation compounds.[11]

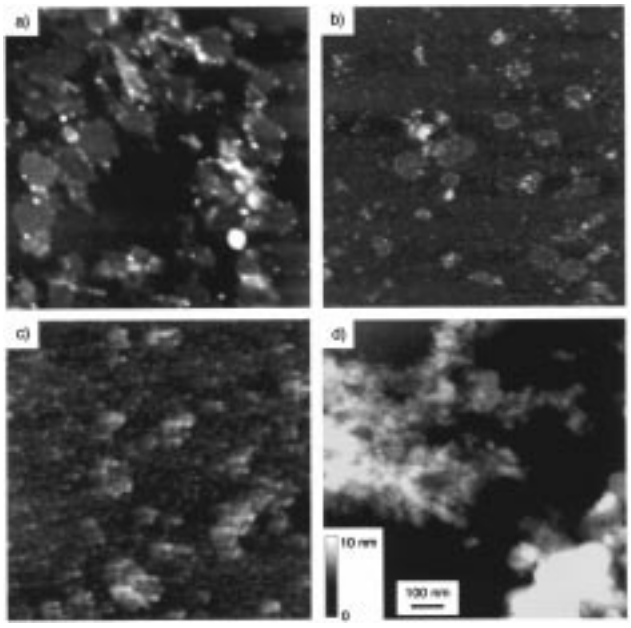

Figure 4. Tapping mode AFM images (1-μm × 1-μm area) of an amine-derivatized silicon surface with adsorbed α-ZrP colloids hydrolyzed at room temperature for (a) 1, (b) 3, and (c) 6 h and (d) at 75 °C for 1 h. The amount of hydrolysis product at the edges of the sheets increases progressively in panels a−c. The temperature dependence of the hydrolysis rate is evident by comparing panel a with panel d.

AFM and TEM images of semicrystalline α-ZrP exfoliated by TBA^+OH^- provide clear evidence that the base hydrolysis reaction proceeds from the edges inward. Figure 4 shows AFM images of α-ZrP colloids adsorbed on amine-functionalized, polished silicon surfaces. Images a−c were obtained from colloidal samples adsorbed after 1, 3, and 6 h of reaction with TBA^+OH^- at 22 °C, respectively. Samples reacted for 1 h show single exfoliated sheets with distinct 1−10-nm high "bumps" around their edges. Most of these smaller features are still associated with the sheets after 1 h, and there are relatively few adsorbed to the silicon surface in between. After 3 h (image b), there are fewer sheets and more small particles, which adhere to the substrate between the sheets. After 6 h (image c), the surface is almost completely covered with these smaller particles, and only a few sheets, which have highly corrugated edges, are observable within the 1- × 1-μm scan area.

The AFM images reveal only the fraction of the colloid that adsorbs to the substrate and may not accurately reflect the overall composition of the suspension itself. However, TEM images of the suspensions, which are more likely to be representative, display similar features (Figure 5). The edges of partially hydrolyzed sheets (Figure 5a) have higher TEM contrast than the inner areas, implying that the features seen on the edges are thicker and/or have higher electron density. This is consistent with the loss of less electron-dense phosphate groups and the formation of a zirconium-rich three-dimensional material, as described by reaction 1. Judging from the gradual formation of the electron-dense small particles on the sheet edges, it is reasonable to assume that the latter consist of hydrated zirconium oxide, the ultimate product of the hydrolysis reaction.

The degree of colloid hydrolysis was quantified by first acidifying the solution to effect restacking, so that the remaining sheets and small zirconia particles could be physically separated from the supernatant and each phase could be analyzed separately. Our experience is that the solid and liquid phases

(19) Avrami, M. *J. Chem. Phys.* **1939**, *7*, 1103; **1940**, *8*, 212; **1941**, *9*, 177.

(20) (a) Clearfield, A.; Tindwa, R. M. *J. Inorg. Nucl. Chem.* **1979**, *41*, 871. (b) Tindwa, R. M.; Ellis, D. K.; Peng, G.-Z.; Clearfield, A. *J. Chem. Soc., Faraday Trans.* **1985**, *181*, 545. (c) Xu, J.; Tang, Y.; Zhang, H.; Gao, Z. *J. Incl. Phenom. Mol. Recognit. Chem.* **1997**, 27, 303.

(21) Kim, H.; Keller, S. W.; Mallouk, T. E.; Decher, G.; Schmitt, J. *Chem. Mater.* **1997**, *9*, 1414.

(22) Alberti, G.; Giontella, E.; Murcia-Mascarós, S. *Inorg. Chem.* **1997**, 36, 2844.

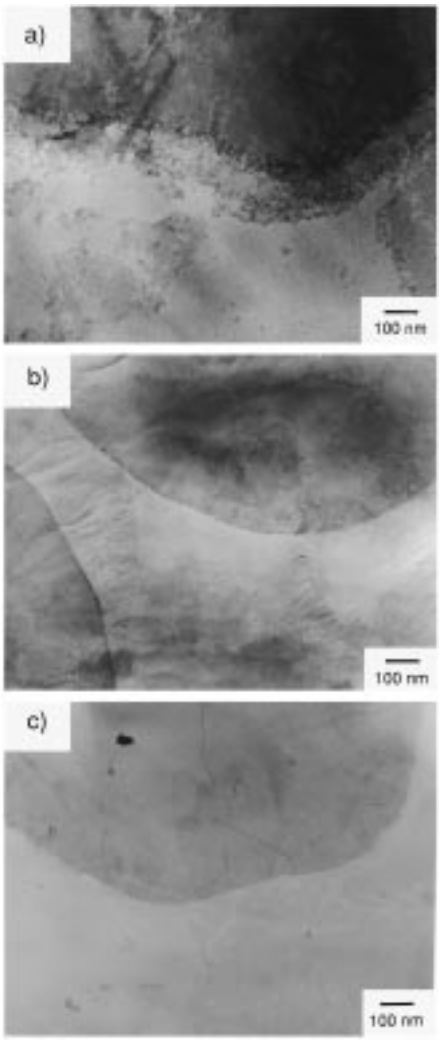

Figure 5. Transmission electron micrographs of exfoliated α-ZrP sheets (a) showing increased contrast at the edges of sheets after 1 h of hydrolysis at room temperature, (b) showing a dramatically reduced hydrolysis rate in the presence of 0.1 M added phosphate after 1 h at room temperature, and (c) showing no apparent edge hydrolysis after 1 h of exfoliation at 0 °C.

cannot be completely separated by centrifugation unless the former is first restacked by acidification. Analysis of both the solid and liquid phases for Zr and P verified that the phosphorus released into the liquid phase was entirely orthophosphate. The acidified liquid phase contained negligible amounts of Zr, in contrast to previous reports of soluble Zr in amine-exfoliated suspensions.[20c]

Figure 6 depicts the percent hydrolysis (defined as 100(1 − R/2), where *R* is the P/Zr ratio in the solid phase) as a function of time for the same semicrystalline colloids represented in Figures 4 and 5. In the presence of excess base, the hydrolysis is fairly rapid at first (10−20% after 1 h) but then slows down and ultimately stops at a value of about 35%. The sample ultimately reaches the same degree of hydrolysis whether the base is added in small aliquots (keeping the pH between 8.5 and 10 for most of the reaction) or all at once at the beginning of the reaction. This behavior suggests that the final value of 35% hydrolysis represents a dynamic equilibrium in reaction 1. Two additional experiments confirmed this hypothesis. First, a sample that had reached hydrolytic equilibrium was precipitated with acid and separated by centrifugation from the supernatant solution that contained the phosphate liberated in

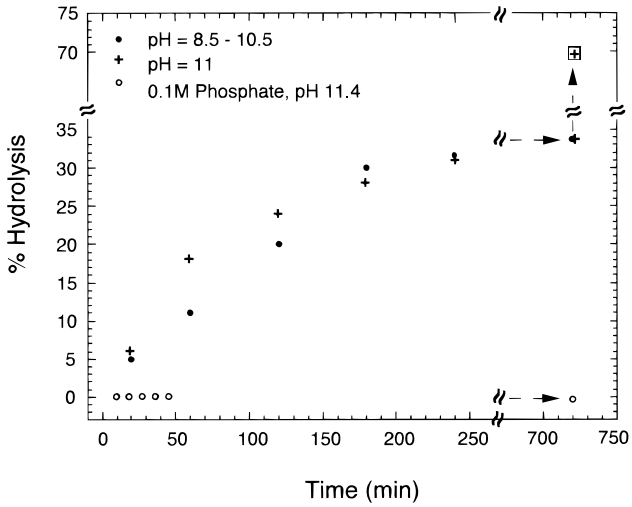

Figure 6. Percent hydrolysis vs time for semicrystalline α-ZrP, exfoliated in aqueous TBA^+OH^- at pH = 8.5−10.5 (●), at pH = 11 (+), and at pH = 11.4 with 0.1 M phosphate (○). The hydrolysis reaction, even at elevated pH, proceeds only to 35% within ∼240 min and is arrested by addition of phosphate. The data point in the upper right (⊞) is from an α-ZrP colloid that has reestablished base hydrolysis equilibrium after the solution phase (containing phosphate from 35% hydrolysis) was replaced by a fresh pH = 11 TBA^+OH^- solution.

the reaction. The solid fraction was again exfoliated in a fresh TBA^+OH^- solution, and the hydrolysis reaction rapidly resumed, ultimately reaching a value of ∼70%. Second, α-ZrP was exfoliated in a solution prepared by reacting phosphoric acid with TBA^+OH^-, to make a pH 11.4 solution that contained 0.1 M phosphate. In the colloid produced from this solution, the P/Zr ratio in the restacked solid was 2.0, even after several days of reaction at 22 °C. TEM images (Figure 5b) showed no evidence of hydrolysis at the edges of the sheets.

These experiments suggest a dynamic equilibrium in which phosphate and hydroxide ions exchange rapidly at the edges of the α-ZrP sheets. The rate of the hydrolysis reaction can be changed dramatically by adding or removing the product (orthophosphate) of the reaction. Chemically, it is reasonable that phosphate groups on the edges should be more reactive than those in inner regions of the sheets because the latter are bonded through three oxygens to zirconium ions. Edge phosphates are likely to have one or more "dangling" P−O or P−OH groups, chemically similar to the exchangeable phosphate groups in γ-ZrP, which bind to zirconium through only two of their oxygen atoms.

It is also apparent from these experiments that the base hydrolysis and exfoliation reactions of α-ZrP are not necessarily connected. As two distinct chemical reactions, it is reasonable to expect that they might have different activation energies. The temperature dependence of the hydrolysis rate (Figure 7) demonstrates that this is, indeed, the case. At all temperatures, the exfoliation reaction is quite rapid. However, the degree of hydrolysis, measured after 1 h, varies considerably with temperature. The most dramatic effect in this regard is the slowing of the hydrolysis reaction to an imperceptible rate at 0 °C. After 3 days at 0 °C, the P/Zr ratio in the solid is 2.0, the concentration of free phosphate in the solution is below the detection limit of the phosphomolybdic acid technique,[12] and the edges of the sheets again show no sign of hydrolysis in TEM images (Figure 5c). On the other hand, samples heated to 75 °C show extensive hydrolysis in AFM images (Figure 4d), relative to identical samples kept at 22 °C.

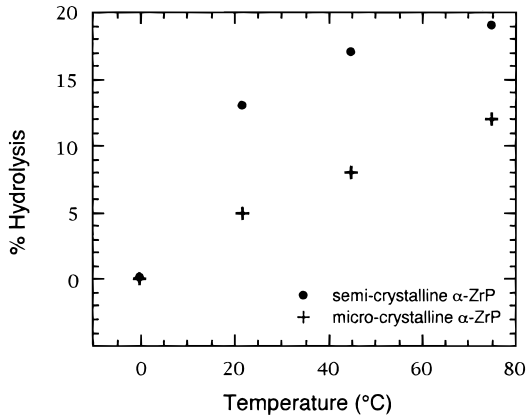

Figure 7. Percent hydrolysis versus temperature for semicrystalline (●) and microcrystalline (+) α-ZrP exfoliated in aqueous TBA^+OH^- at pH = 10.5 for 1 h. The hydrolysis rate is essentially zero at 0 °C.

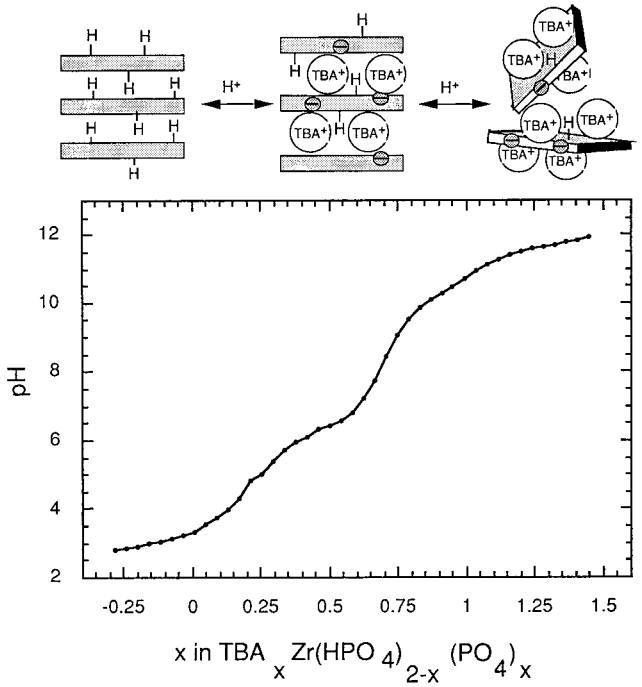

Figure 8. Titration of exfoliated semicrystalline α-ZrP with HCl at 0 °C.

It has been noted that colloids made by exfoliating highly crystalline α-ZrP hydrolyze more slowly than those derived from less crystalline materials.[20] Figure 7 shows the difference in the hydrolysis rates of microcrystalline and semicrystalline α-ZrP colloids. While a quantitative analysis of this difference is difficult because of the dispersity in crystallite size, the faster reaction of less crystalline materials is easily understood in light of the microscopic observation of edge hydrolysis. For both large and small sheets, the exfoliation reaction is fast, and so all phosphate groups are quickly exposed to the basic solution. However, only those phosphate groups at the edge are reactive, and because smaller sheets have a larger edge-to-area ratio, their initial rate of hydrolysis is greater.

Restacking of Hydrolysis-Free Colloids. The availability of hydrolysis-free α-ZrP colloids makes it possible to study the exfoliation/restacking equilibrium without the complication of side reactions. Figure 8 depicts an acid titration curve, obtained at 0 °C, for a colloid prepared by reacting microcrystalline α-ZrP with excess TBA^+OH^-. More than one equivalence point is apparent, resembling the pH-dependent ion exchange capacity of α-ZrP with various intercalates.[23] The pH varies without any apparent endpoint at the acidic end of the curve, corresponding to a variable TBA^+ loading in the intercalation compound $(TBA)_xZr(HPO_4)_{2-x}(PO_4)_x{\cdot}nH_2O$. Previous studies have demonstrated that the first-stage bulk intercalation compound has a stoichiometry of $x \approx 0.35-0.50$.[24] Colloidal suspensions that were examined by AFM and TEM at $x < 0.5$ revealed a significant fraction of restacked α-ZrP. The rise in pH to the basic side of this composition corresponds to the exfoliation equilibrium, and the inflection point ($x = 0.7$, pH 8.4) represents the stoichiometry of the fully exfoliated solid. AFM images of colloids with $x \geq 0.7$ adsorbed on silica surfaces (see below) revealed exclusively single sheets.

Interestingly, a second inflection point appears in the titration curve at $x = 1.0$, pH 10.7, possibly signaling the formation of a different unilamellar colloidal phase. At $x = 1.0$, there should be a densely packed monolayer of TBA^+ ions on either side of each α-ZrP sheet.[21] The $x = 0.7$ phase corresponds to a more loosely packed $TBA^+/ZrP/TBA^+$ sandwich structure, in which the average area per TBA^+ ion on each side of the ZrP sheet is ca. 70 $Å^2$.

Tiling of Cationic Surfaces by α-ZrP Sheets. Perhaps the most remarkable effect of eliminating the α-ZrP base hydrolysis reaction is the quality of self-assembled monolayers of sheets that grow on amine-terminated silicon surfaces. With partially hydrolyzed samples, the surface coverage is rather patchy (Figure 4), and small particles, which are presumably hydrated zirconium oxide, fill in the gaps between sheets. Figure 9 shows the coverage of the same substrates by micro- and semicrystalline α-ZrP colloids exfoliated for 1 h at 0 °C and $x = 0.77$, pH 9.5. In both cases, there are some small regions of uncovered substrate and a small fraction of the surface with bilayer coverage. However, for both colloids, the surface is predominantly covered by a single layer of sheets, and the total surface coverage is in excess of 90%. The very efficient tiling and avoidance of overlaps suggests that, at least during the adsorption process, the sheets must have some lateral mobility on the surface.

Individual sheet dimensions for microcrystalline α-ZrP range from 100 nm to more than 2 μm, all with irregular shapes. The thickness of these sheets was found by AFM to be 8−10 Å, consistent with previous ellipsometric and diffraction measurements from multilayer films[21] and with the crystallographic layer thickness of α-ZrP.[14] For the semicrystalline colloid, the lateral size distribution is much narrower (80−120 nm), and the corners of many of the sheets reflect the pseudohexagonal in-plane symmetry of α-ZrP. The apparent thickness of the semicrystalline monolayer was consistently slightly higher (12−15 Å) than that derived from microcrystalline α-ZrP. Clearfield et al. have proposed that not all of the phosphate groups in the semicrystalline material are in their equilibrium positions. This effect could contribute to the difference in thickness determined by AFM.[25]

Selective Functionalization of the Edges of α-ZrP Sheets. The reversibility of the hydrolysis equilibrium (eq 1) can be adapted to specifically functionalize the edges of colloidal α-ZrP sheets by substituting an appropriate phosphonate linker molecule for inorganic phosphate. This is illustrated in Figure 10, which shows TEM images of colloids incubated with vinylphosphonic acid and OsO_4, and control samples containing eth-

(23) Amphlett, C. B. *Inorganic Ion Exchangers*; Elsevier Publishing Co.: London, England, 1964; p 106.
(24) Garcia, M. E.; Naffin, J. L.; Deng, N.; Mallouk, T. E. *Chem. Mater.* **1995**, *7*, 1968.
(25) Clearfield, A.; Oskarsson, C. *Ion Exch. Membr.* **1972**, *1*, 91.

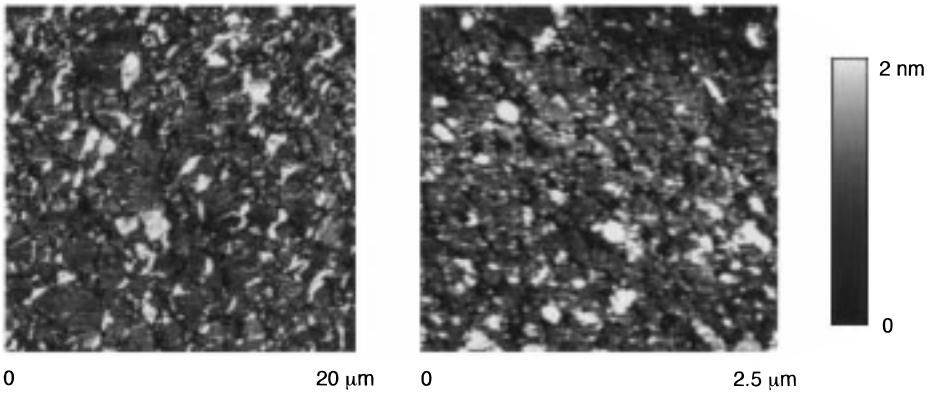

Figure 9. Tapping mode AFM images of hydrolysis-free microcrystalline (left) and semicrystalline (right) α-ZrP monolayers, adsorbed onto amine-derivatized silicon substrates at 0 °C.

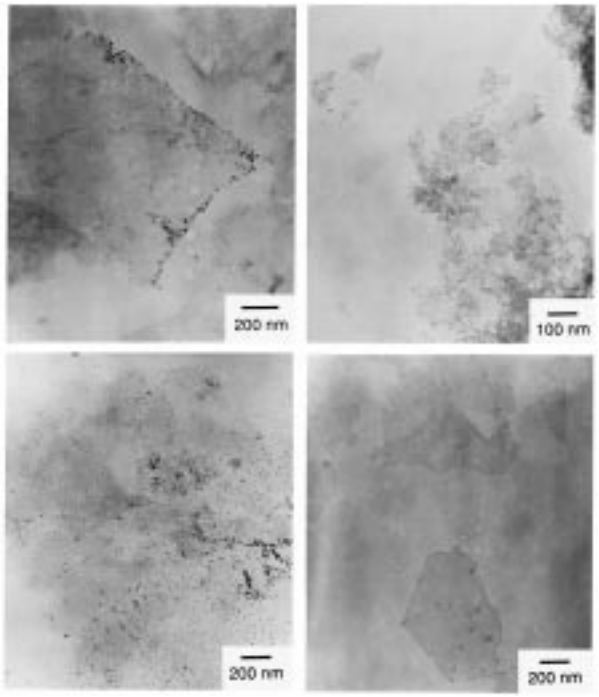

Figure 10. TEM images of exfoliated α-ZrP reacted with OsO_4 and vinylphosphonic acid (top) and with OsO_4 and ethylphosphonic acid (bottom). The sample in the top right shows semicrystalline and the others show microcrystalline α-ZrP colloids. The top images show colloidal OsO_2 attaching selectively to the edges of sheets. The control experiments with ethylphosphonic acid show regions where there are OsO_2 particles (bottom left) and α-ZrP sheets (bottom right) but no selective binding of particles to the edges of the sheets.

ylphosphonic acid and OsO_4. The colloids were prepared at 22 °C in the presence of the phosphonic acids to allow the exchange reaction to proceed, with the pH fixed at 10.5−11. For both microcrystalline and semicrystalline materials, 2.2 mol of phosphonic acid and 0.2 mol of OsO_4 were used per mole of α-ZrP.

When vinylphosphonate is exchanged for phosphate, the edges of the sheets become decorated with olefinic groups. OsO_4 reacts at these sites and gradually forms 2−20-nm-diameter osmium(IV) oxide (presumably $OsO_2 \cdot 2H_2O$) colloids,[26] which are evident in the TEM images. For large sheets prepared from microcrystalline α-ZrP, the edges are almost entirely decorated by these electron-dense features. The $OsO_2 \cdot 2H_2O$ particles also adhere exclusively to the edges of aggregates of sheets prepared from semicrystalline α-ZrP. In this case, however, there is too little $OsO_2 \cdot 2H_2O$ in the sample to decorate the sheet edges extensively. Approximating each semicrystalline α-ZrP sheet as a 1-nm-thick disk with a diameter of 120 nm, there are on the order of 1000 exchangeable phosphate groups at the edge of each sheet, and about 45 000 $Zr(HPO_4)_2$ formula units per sheet. The $OsO_2 \cdot 2H_2O$ particles (approximated as 5-nm-diameter spheres) each contain about 600 Os atoms. This rough calculation gives about 20 particles per sheet (or about 1 particle for every 60 edge phosphate groups) in the case of the semicrystalline α-ZrP. This is consistent with the top right image in Figure 10, which shows particles dotting the edges of semicrystalline α-ZrP. The average diameter of the microcrystalline α-ZrP sheets is about 10 times that of the semicrystalline material, which by the same calculation gives about 1 particle per 6 edge phosphate groups. In this case, there is enough $OsO_2 \cdot 2H_2O$ to cover the edges of the sheets quite densely, as seen in the top left image of Figure 10. While there is a previous observation of nanoparticles decorating the edges of clay colloids, in that case the particle−sheet interaction was a simple electrostatic one.[5] Figure 10 shows that it is possible to derivatize the edges of α-ZrP sheets selectively, by means of covalent bonds.

The lower half of Figure 10 depicts TEM images from a control experiment carried out with ethylphosphonate and microcrystalline α-ZrP. In the presence of organic molecules, OsO_4 is also reduced to give osmium(IV) oxide particles,[27] but in this case there are no olefinic groups present to tether these particles to the edges of the sheets. In some regions of the sample (image at bottom left), $OsO_2 \cdot 2H_2O$ particles are apparent, but they are not specifically associated with the edges of sheets. In other regions (bottom right), α-ZrP sheets are found, but they are not associated with $OsO_2 \cdot 2H_2O$. Sharp edges on the exfoliated sheets in the image at the bottom right illustrate that added ethylphosphonate, like added phosphate, inhibits the base hydrolysis reaction at the edges of the α-ZrP sheets.

Conclusions

This study has demonstrated that the edges of colloidal sheets of α-ZrP, a prototypical lamellar phosphate, have very different reactivity than inner regions of the same sheets. The dangling phosphate groups on these edges are susceptible to exchange

(26) Behrman, E. J. In *The Science and Biology of Specimen Preparation for Microscopy and Microanalysis*; Revel, J.-P., Barnard, T., Haggis, G. H., Eds.; Scanning Electron Microscopy, AMF: O'Hare, IL, 1984; pp 1−5.

(27) Hayat, M. A. *Fixation for Electron Microscopy*; Academic Press: New York, 1981; pp 178−179.

by hydroxide, and this is the source of the base hydrolysis reaction of α-ZrP. The exchange is an equilibrium process, which may be driven in one direction or the other using Le Chatelier's principle. This conclusion unifies several previous observations of base hydrolysis. It explains why smaller crystallites hydrolyze faster than larger ones,[28] and why the hydrolysis reaction is always incomplete in the presence of excess base. A certain amount of base hydrolysis has been found to be beneficial in the preparation of "pillared" restacked α-ZrP colloids. This effect has been interpreted in terms of porosity induced by hydrolysis within the sheets.[29] In light of the results presented here, it is more likely that the pillaring effect arises because zirconia particles a few nanometers in diameter are formed at the edges of the sheets, and restacking produces porosity at these "bumpy" edges.

The fact that the hydrolysis reaction can be effectively shut off by lowering the temperature, or by adding phosphate or phosphonates to the solution, allows one to obtain clean acid−base titration curve of α-ZrP colloids. It is possible that the same strategies might be effective in preparing hydrolysis-free colloids of some of the other lamellar phosphates (e.g., Ti, Sn) which are more susceptible to base hydrolysis than α-ZrP. Further, self-assembled monolayers of sheets of unprecedented quality can be prepared from hydrolysis-free α-ZrP colloids, and the edges of the sheets can be rationally derivatized by means of phosphonates. These results may have significant implications for the preparation of self-assembled multilayer films and nanocomposite materials from layered metal phosphates.

Acknowledgment. This work was supported by a grant from the National Science Foundation (CHE-9529202).

JA9818710

(28) Clearfield, A.; Stynes, J. A. *J. Inorg. Nucl. Chem*. **1964**, *26*, 117.

(29) (a) Alberti, G.; Costantino, U.; Marmottini, F.; Vivani, R.; Zappelli, P. In *Pillared Layered Structures: Current Trends and Applications*; Mitchell, I. V., Ed.; Elsevier: London, 1991; p 119. (b) Maireles-Torres, P.; Olivera-Pastor, P.; Rodriguez-Castellon, E.; Jimenez-Lopez, A.; Tomlinson, A. A. G. *J. Solid State Chem.* **1991**, *94*, 368. (c) Maireles-Torres, P.; Olivera-Pastor, P.; Rodriguez-Castellon, E.; Jimenez-Lopez, A.; Alagna, L.; Tomlinson, A. A. G. *J. Mater. Chem.* **1991**, *1*, 319.